Available online at www.sciencedirect.com
ScienceDirect
Journal of Magnetism and Magnetic Materials 320 (2008) 1272–1281
Journal of magnetism and magnetic materials
www.elsevier.com/locate/jmmm

Current Perspectives

Current-induced domain wall motion

G.S.D. Beach*, M. Tsoi, J.L. Erskine

Department of Physics, The University of Texas at Austin, Austin, TX 78712 0264, USA

Received 27 September 2007; received in revised form 13 October 2007
Available online 28 December 2007

Abstract

The present understanding of domain wall motion induced by spin-polarized electric current is assessed by considering a subset of experiments, analytical models, and numerical simulations based on an important model system: soft magnetic nanowires. Examination of this work demonstrates notable progress in characterizing the experimental manifestations of the "spin-torque" interaction, and in describing that interaction at a phenomenological level. At the same time, an experimentally verified microscopic understanding of the basic mechanisms will require substantial future efforts, both experimental and theoretical.

PACS: 75.60.Ch; 85.75.−d; 75.75.+a

Keywords: Spin-transfer torque; Domain wall dynamics; Ferromagnetic nanowires

1. Introduction

In 1978, Luc Berger predicted that a spin-polarized current should apply a torque to a magnetic domain wall [1]. In a series of remarkable but only recently appreciated works, Berger set the theoretical [1–4] and experimental [5–7] groundwork for what is now a burgeoning industry in magnetism research. This article will present our perspectives on what progress has been made in the intervening years and what key questions remain unanswered. This is by no means an exhaustive review of current-induced domain wall motion (CIDWM). Rather, it is an attempt to identify inconsistencies and unresolved issues so as to assess the present state of understanding and help guide future efforts.

We shall focus on the current-driven motion of domain walls in submicron "wires" fabricated from soft magnetic thin films. The scope of the assessment is limited to examining a subset of work that highlights key experimental results and their interpretation within existing models. This paper is organized into three sections. Section 2 outlines general features of domain wall physics as described by the most prominent phenomenological models. The aim is to summarize the predicted effects of spin-polarized current on domain walls in terms of specific model parameters, without delving into the microscopic justifications for those parameters. Section 3 then focuses on experiments that have probed various aspects of spin-transfer torque (STT) and domain walls, describing what the experiments do tell us and, just as important, what they do not. Finally, Section 4 attempts to put these experimental results into perspective.

2. Spin torque and domain walls

CIDWM has been documented in materials ranging from magnetic semiconductors [8] to perpendicular-anisotropy superlattices [9], but the most widely studied material by far has been Permalloy ($Ni_{80}Fe_{20}$). A combination of desirable properties, including low anisotropy and near-zero magnetostriction, has led to its decades-long ubiquity in magnetic storage technology. As a result, it is among the best-characterized magnetic alloys and has become a benchmark system in magnetization dynamics studies.

Early work in CIDWM involved domain walls in extended films, but in recent years, the focus has shifted to "nanowires". In addition to their potential role in future

*Corresponding author. Tel.: +1 512 471 7073.
E-mail address: gbeach@physics.utexas.edu (G.S.D. Beach).

0304-8853/$ - see front matter © 2007 Elsevier B.V. All rights reserved.
doi:10.1016/j.jmmm.2007.12.021

devices, ferromagnetic nanowires offer greater control of domain walls, they are ideally suited to carrying current, and their dimensions are amenable to numerical studies. In these structures, magnetic domains lie along the wire axis, and are separated by head-to-head or tail-to-tail domain walls. The spin structures within these walls are reasonably well understood, and approximate analytical models describing their dynamics were derived long ago [10]. Where the analytical models fail, numerical integration of the Landau–Lifshitz–Gilbert (LLG) equation takes over in providing further insight. LLG simulations have shown that domain walls in nanowires can exhibit relatively simple or highly complex behavior, and some of this behavior has been borne out by experiment.

The effects of electric current have been treated by the addition of two current-induced torque terms to the LLG equation [11–15]. This section will outline the phenomenology of domain wall motion in nanowires and the roles played by these torques. As we write from an experimental point of view, we take a heuristic approach to the theory with the aim of identifying the observable manifestations of STT on domain wall motion. This section will serve as a guide for a later critical analysis of experiments.

2.1. Forms of spin torque

With current density j along $\hat{\mathbf{x}}$, the time evolution of the (normalized) magnetization vector $\mathbf{m}$ may be described by the LLG equation:

$$\dot{\mathbf{m}} = -\gamma \mathbf{m} \times \mathbf{H}_{eff} + \alpha \mathbf{m} \times \dot{\mathbf{m}} - v_j \frac{\partial \mathbf{m}}{\partial x} + \beta v_j \mathbf{m} \times \frac{\partial \mathbf{m}}{\partial x}. \quad (1)$$

The first term on the right accounts for torque by the effective field $\mathbf{H}_{\text{eff}}$ (including applied, demagnetizing, anisotropy, and exchange fields). The second term describes (Gilbert) damping torque, parameterized by a dimensionless α. The final two terms, where $v_j = \eta j$, express current-induced torques on $\mathbf{m}$ about two mutually orthogonal axes in a region of nonuniform magnetization. These torques are most commonly termed *adiabatic* and *nonadiabatic*, respectively [11–16], and the parameters η and β characterize their strength.

The most widely agreed upon interaction between a spin-polarized current and a domain wall is adiabatic STT [1,11,12,14]. A conduction electron traversing a domain wall experiences a torque that compels its spin to follow the local magnetization direction. In so doing, its spin "flips" as it crosses a wall separating two opposing domains. In this adiabatic process, the consequent change in electron spin angular momentum is transferred to the (localized) spins within the wall. The torque associated with this spin transfer is the adiabatic term in Eq. (1). Berger's original description [1], as well as most subsequent work [11,12,14], arrives at

$$\eta = \frac{g\mu_B P}{2eM_s}. \quad (2)$$

Here g, μ_B, and e are the Landé factor, Bohr magneton, and electron charge, respectively, M_s is the saturation magnetization, and P is the conduction electron spin polarization. For Permalloy, $\eta = P \times 7 \times 10^{-11}\,\text{m}^3/\text{C}$, or a velocity of $P \times 7\,\text{m/s}$ per $10^{11}\,\text{A/m}^2$ of current. The value of P is not well known, but estimates range from 0.4 to 0.7.

The microscopic basis for including the nonadiabatic term in Eq. (1) is more controversial. Berger first introduced such a term as a consequence of the Stern–Gerlach force on conduction electrons by the gradient in the s–d exchange field [2]. This term may also arise from linear momentum transfer [11], spin-flip scattering [13], or directly from adiabatic STT if Lifshitz-type damping, rather than the Gilbert form, is used [16]. Here we treat it simply as a parameter to be determined by experiment.

2.2. Domain wall structures in nanowire geometries

Given the equation of motion equation (1), the next step is to apply it to a domain wall. A "nanowire" as defined here is a planar ferromagnetic stripe of length L, width w, and thickness t along $\hat{\mathbf{x}}$, $\hat{\mathbf{y}}$, and $\hat{\mathbf{z}}$, respectively, with $L \gg w > t$. The structure of a wall depends on a balance between exchange and anisotropy energies. The former is minimized when spins lie parallel to one another; the latter encourages alignment along a preferred axis. In soft magnetic materials such as Permalloy, shape anisotropy dominates, and domains lie along the wire axis. Walls separating antiparallel domains come in two topologies: transverse and vortex. The transverse wall of Fig. 1(a), in which $\mathbf{m}$ rotates continuously across the wall, efficiently minimizes exchange energy at the expense of free magnetic poles at the edges. The resulting magnetostatic energy grows with w and t. As either of these dimensions increases, the system eventually favors a "closure" structure such as the vortex wall of Fig. 1(b), in which the magnetization circulates in the plane about a small perpendicular "vortex core." This configuration minimizes free poles but increases exchange energy. By comparing the magnetostatic energy of a transverse wall to the additional exchange energy associated with a vortex, McMichael and Donahue [17], and later Nakatani et al. [18], arrived at a phase boundary $w \cdot t \approx 60 L_{ex}^2$ (Fig. 1c), where the exchange length $L_{ex} \approx 5\,\text{nm}$ for Permalloy. TWs are stable in thin, narrow wires, but VWs are preferred as either dimension is increased. Modern magnetic imaging techniques have provided experimental verification of these wall structures and their relative energies [19].

2.3. Transverse domain walls: the one-dimensional approximation

Transverse domain walls are the simplest to treat analytically, using a one-dimensional wall approximation whose equations of motion are well known [10]. In this model, $\mathbf{m}$ rotates from $-\hat{\mathbf{x}}$ to $+\hat{\mathbf{x}}$ over a characteristic distance Δ, inclined from the easy plane by an angle ψ

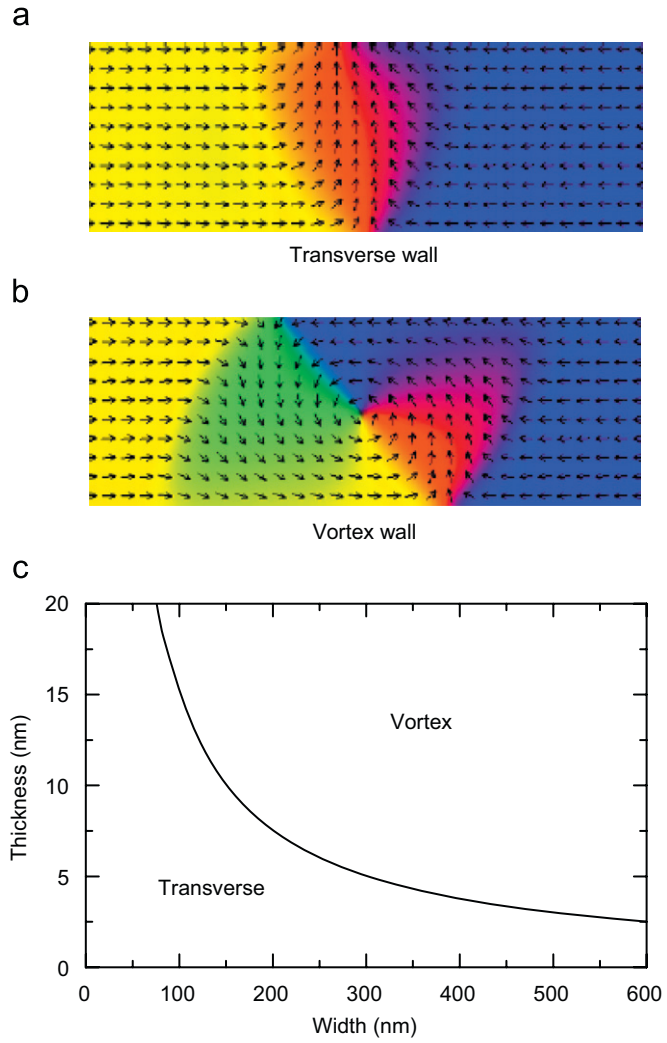

Fig. 1. Spin structures of (a) transverse and (b) vortex domain walls. Which of these structures yields the lowest total energy is a function of the aspect ratio, described by the phase boundary in (c).

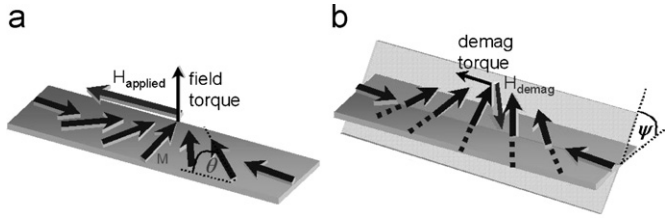

Fig. 2. Schematic of a one-dimensional domain wall and the torques involved in driving its motion.

(see Fig. 2). An applied field H along $\hat{\mathbf{x}}$ exerts a torque that cants the wall spins out of the plane, generating a demagnetizing field H_d. The demagnetizing torque, $\gamma\mathbf{M}\times\mathbf{H}_d$, then cants the spins towards the applied field, driving the wall forward. The wall velocity v depends on H_d which, unlike H, has a finite limit: at $\psi\approx\pi/4$, the demagnetizing torque, and thus v, peaks. If H drives ψ past this limit, the wall plane can no longer remain stationary, a transition termed Walker breakdown [20]. Instead, the wall plane precesses, causing the demagnetizing torque and instantaneous velocity to change direction with each quarter-period, with a time average approaching zero. ψ rotation becomes more rapid with increasing H, leading to a small net damping torque $(\alpha\mathbf{M}\times\dot{\mathbf{M}})$ that cants the wall spins toward the applied field, driving forward motion. At high H, damping torque provides the dominant net contribution to v.

With current included, Eq. (1) can be solved analytically [14] to yield a threshold for precession

$$H_W^{1D}(j) = H_{W0}^{1D} + \left(\frac{\eta}{\mu}\right)\left(1-\frac{\beta}{\alpha}\right)j, \tag{3}$$

below and far above which the influences of H and j on v are separable and asymptotically linear [21]:

$$v_I^{1D} = \mu H + \frac{\beta}{\alpha}\eta j, \tag{4a}$$

$$\langle v_{II}^{1D}\rangle \to \alpha^2\mu H + \eta j, \tag{4b}$$

respectively. The mobility μ and zero-current Walker field H_{W0}^{1D} are given by

$$H_{W0}^{1D} = \tfrac{1}{2}\alpha H_K^{\perp}, \tag{5a}$$

$$\mu = \gamma\Delta/\alpha. \tag{5b}$$

Both are functions of the anisotropy, which in a Permalloy nanowire is dominated by shape. The shape anisotropy constants $K_u^{||}$ and $K_u^{\perp}$ along $\hat{\mathbf{y}}$ and $\hat{\mathbf{z}}$, respectively, for an infinitely long wire with aspect ratio $p = w/t$ are [22]

$$K_u^{||}/M_s^2 = 4\arctan p^{-1} + p^{-1}\ln(1+p^2) - p\ln(1+p^{-2}) \tag{6}$$

and $K_u^{\perp} = 2\pi M_s^2 - K_u^{||}$. These two anisotropies play very important roles, and it is important to keep in mind their magnitude. For a Permalloy nanowire with $w/t = 10$, the corresponding anisotropy fields $H_K = 2K_u/M_s$ along $\hat{\mathbf{y}}$ and $\hat{\mathbf{z}}$ are approximately 1 and 9 kOe, respectively. The induced anisotropies in continuous thin films of Permalloy, for comparison, are typically on the order of a few Oe.

2.4. Limitations of the one-dimensional model

The 1D model is helpful in visualizing how field and current drive domain wall motion, and it qualitatively reproduces much of the behavior seen experimentally [23]. As a result this model has been widely used as a foundation in building the theory of current-driven wall motion. However, as recently pointed out [21], the 1D model exhibits serious quantitative shortcomings in describing real systems. In this section, we briefly compare the predictions of the field-driven 1D model to experiment.

Fig. 3(a) shows the average wall velocity versus field at $j = 0$, as computed from the full solution to the 1D model. Anisotropy constants were computed via Eq. (6) for a 500 nm × 20 nm Permalloy stripe, with $\alpha = 0.02$. For

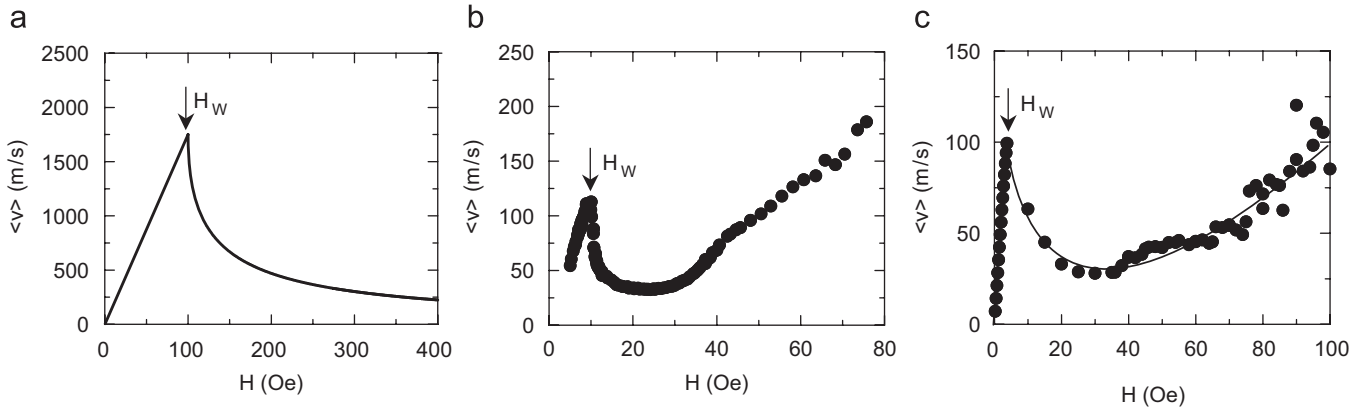

Fig. 3. (a) Mobility curve for a 500 nm by 20 nm Permalloy wire, calculated using the 1D model. (b) Measured mobility curve for a 490 nm × 20 nm Permalloy nanowire. (c) Mobility curve computed using LLG numerical simulations for a 200 nm × 20 nm Permalloy wire (line is a visual guide). Note different axis scales for each figure.

comparison, the experimentally measured [24] mobility curve of a 490 nm × 20 nm Permalloy nanowire is shown in Fig. 3(b). Several striking differences are immediately apparent. Most notable are the differences in scale, both in field and velocity. The 1D model exhibits viscous motion up to a breakdown field of ~100 Oe, at which the velocity is in excess of 1700 m/s. By contrast, the measured breakdown field is ~9 Oe, with a critical velocity of only ~110 m/s.

In the 1D model, the breakdown transition occurs when the field torque is great enough to periodically reverse the sense of the domain wall. This reversal involves a rather large energy barrier: the demagnetizing field that arises when the wall plane cants at a large angle. As has been seen in micromagnetic simulations [25], this barrier can be "bypassed" by the nucleation of a vortex, even in geometries in which a vortex is not the energetically favorable ground state. Rather than simple precession, these simulations reveal a dynamic evolution of the domain wall structure above the critical field [25]. Beginning with a transverse structure, a vortex core is nucleated at the apex of the wall, and it moves across the width of the wire. As the vortex moves laterally, the wall first moves forward and then begins to move backward after the vortex passes the wire midpoint. When the vortex reaches the other side, a transverse-like wall is recovered, but its sense is reversed. Because the energy required to nucleate the vortex is much less than that required for large-angle wall precession, the onset of oscillatory wall motion occurs at far lower field.

As might be expected, micromagnetic simulations of wall dynamics come much closer to describing experimental observations than does the 1D model. As an example, Fig. 3(c) shows the average velocity versus field simulated numerically [26,27] for a 200 nm × 20 nm Permalloy stripe. In the simulation, vortex-mediated precessional motion occurs as just described for fields above ~7 Oe. A comparison with the data of Fig. 2(b), though qualitative given the different dimensions, shows a marked improvement over the 1D model in describing experimental observations. These results emphasize that the relevant scales in energy, field, and velocity depend in a critical way on the microscopic details of the wall structure.

2.5. Vortex domain walls and equivalent forces

A proper understanding of experiments requires explicit treatment of vortex domain walls [4,28–31]. Any model of vortex wall dynamics is necessarily 2D, as describing the wall position requires two coordinates: its location along the stripe axis (along $\hat{\mathbf{x}}$), and the lateral position of the core within the wall (along $\hat{\mathbf{y}}$). The velocity is thus a vector $\mathbf{v}$ with components $v_{||}$ and $v_{\perp}$ along $\hat{\mathbf{x}}$ and $\hat{\mathbf{y}}$, respectively.

Owing to its topology, when a vortex moves along one axis it experiences a "force" along the other. This "gyrotropic force" is related to the Magnus force of fluid dynamics, which arises in a system with nonzero vorticity. Just as for a transverse wall, there are two dynamic regimes of vortex wall motion. Viscous translation, similar to the motion of a 1D wall below H_{W}, occurs if the lateral vortex coordinate remains fixed ($v_{\perp} = 0$) as the wall moves. $v_{\perp} \neq 0$ marks a gyrotropic regime in which lateral vortex motion plays a role analogous to wall plane precession in the 1D model.

Vortex wall motion is most conveniently treated using an equivalent form of Eq. (1) first introduced by Thiele [28]. This alternate language translates torques on individual spins into "forces" on a composite spin structure. For our purposes, it is most conveniently written in component form [4,29]:

$$x : (D_{xx})v_{||} - (G)v_{\perp} = -\left(\frac{\beta}{\alpha}D_{xx}\right)\eta j - F_x^{\mathrm{H}},$$
$$y : (G)v_{||} + (D_{yy})v_{\perp} = -(G)\eta j - F_y^{\mathrm{H}}. \quad (7)$$

The dissipation tensor D_{ij} describes "viscous" forces that tend to impede wall motion (damping) and "drag" it with a current (nonadiabatic STT). These terms are functions of the wall structure, as described below. When present, a vortex contributes the additional gyrotropic terms in

Eq. (7). Gyrotropic forces arise from the motion of a vortex, $\mathbf{F}_v = \mathbf{G} \times \mathbf{v}$, and from the adiabatic term of Eq. (1), $\mathbf{F}_j = \mathbf{G} \times (\eta \mathbf{j})$. The gyrovector $\mathbf{G}$, given by $\mathbf{G} = \pm(2\pi M_s/\gamma)\hat{\mathbf{z}}$ [4,29], lies along the axis of the vortex core, with a sign that depends on the core polarization. The remaining terms in Eq. (7) account for "external" forces, including Zeeman, $F^H \propto M_s H$, and geometrical "restoring forces". This equivalent force approach provides the basis for generalizing the 1D description in Section 2.3 to describe analytically the dynamics of vortex walls [28–31].

The viscous terms in Eq. (7) derive from the damping term of Eq. (1) and depend on the wall structure $\mathbf{m}(\mathbf{x})$ via

$$D_{ij} = \frac{\alpha M_s}{\gamma} \int dV \frac{\partial \mathbf{m}}{\partial x_i} \cdot \frac{\partial \mathbf{m}}{\partial x_i} \equiv \frac{2M_s w \alpha}{\gamma \Delta_{\text{eff}}^{ij}}, \tag{8}$$

where the Δ_{eff} are generalized "wall width" parameters [18]. Approximate analytical forms for the spin structure of vortex domain walls have been developed [29,30], from which expressions for Eq. (8) may be derived. A vortex is described by two characteristic dimensions: the width of its core ($\sim l_{ex}$) and the outer radius R of the circulating region of in-plane magnetization ($\sim w/2$). If no vortex were present, D_{yy} vanishes and $D_{xx} = 2M_s w\alpha/\gamma\Delta_{TW}$, where $\Delta_{TW} = \sqrt{A/K_u^{||}}$ is the width of a transverse wall (A is the exchange constant). When a wall contains a vortex, it leads to a nonzero $D_{yy} \approx \alpha(\pi M_s/\gamma)\ln(R/l_{ex})$ and modifies D_{xx} by decreasing the effective wall width, with $\Delta_{VW} \approx \Delta_{TW}/(2 + 0.5\ln(R/l_{ex}))$ in the simple model of Ref. [29].

It should be emphasized that the "wall width" parameter of domain wall dynamics is not, in fact, the apparent width of the wall. It is a length scale describing the distance over which the gradient in $\mathbf{m}(\mathbf{x})$ is large. Take the micromagnetically computed [26] wall structures shown in Fig. 1, for example. The walls in these 200 nm × 5 nm Permalloy stripes extend several hundred nm along the stripe, but Δ_{eff} calculated as per Eq. (8) is only ~20 nm and ~40 nm for the vortex and transverse walls, respectively.

3. Experimental manifestations of STT

The previous section described the principal models of domain wall motion and the means by which spin-polarized current can influence that motion. In this section, we describe key experiments that probe the spin-torque interaction and describe what insight they give about the models just described.

3.1. Threshold currents and domain wall depinning

Just as there is a threshold for field-driven magnetization reversal, i.e., the coercivity, there is an experimentally observed threshold j_{th} that a current must exceed to displace a wall. The origin of j_{th} remains unclear, with a central question being whether it is "intrinsic" [11,12,32,33] or "extrinsic" [13,34]. The concept of an intrinsic current threshold originated with Berger [3]. If $\beta = 0$ in Eq. (1), the current-induced torque acts only to cant the spins of a domain wall out of the plane. Once the canting angle reaches equilibrium, the wall stops, even in the absence of pinning. However, if the torque drives the wall plane beyond ~45°, an equilibrium no longer exists. Instead the wall precesses, yielding a sustained net velocity analogous to field-driven motion above Walker breakdown. The "intrinsic" threshold corresponds to the torque necessary to drive precession and is given, in the 1D model, by the breakdown criterion of Eq. (3). At $H = 0$ one has

$$j_{th}^{prec} = \frac{\mu H_{W0}^{1D}}{\eta}. \tag{9}$$

In other words, when the effective electron "velocity" ηj reaches the Walker velocity $v_w = \mu H_W$, current-driven precession ensues and the wall begins to move.

If $\beta \neq 0$ no "intrinsic" threshold exists. In a perfect nanowire, a wall moves with finite velocity for any nonzero j [13]. In this case, pinning is introduced to generate an extrinsic current threshold corresponding to the "force" that current must apply to dislodge a wall from a potential well. By equating the current-induced (nonadiabatic) force on a wall, $f_j = (\beta/\alpha)2M_s\eta j/\mu$ with the "force" due to pinning, $f_p = 2M_s H_p$, one arrives at the "extrinsic" threshold current for a site with an effective pinning field H_p [35]:

$$j_{th}^{pin} = \frac{\mu H_p}{(\beta/\alpha)\eta}. \tag{10}$$

Expressed in terms of wall mobility and critical fields, the thresholds (9) and (10) take essentially the same form. The question then arises as to whether they can be distinguished experimentally. Consider first their expected magnitudes. The 1D model predicts $j_{th}^{prec} \sim 10^{13}\,A/m^2$ for Permalloy nanowires, much higher than the 10^{11}–$10^{12}\,A/m^2$ typically observed. The large discrepancy, widely cited as a failure of the adiabatic STT model, provided a major impetus for the introduction of "nonadiabatic" torques [13,14]. However, it could just as well be interpreted as a failure to properly describe the wall.

The large precessional threshold predicted for a 1D wall is a consequence of the large torque required to tip the wall spins out of the easy plane. As we have seen, the onset of *vortex-mediated* precession demands much less torque. The threshold for field-driven breakdown in nanowires is an order of magnitude lower than is required for rigid precession; the "intrinsic" critical current should likewise be much lower. Indeed, recent $\beta = 0$ micromagnetic calculations for experimentally appropriate geometries [33] found sustained vortex-driven motion at currents on par with experiments, particularly when temperature effects were included. Comparing once again Eqs. (9) and (10), measured Walker fields in nanowires are typically ~5–15 Oe [23,36–38], in the same range as typical pinning fields. Hence the "intrinsic" threshold current expected for $\beta = 0$ is of the same order as the "extrinsic" threshold expected for $\beta \sim \alpha$. Despite frequent statements to the contrary, the "low" experimental threshold currents

cannot be taken alone as evidence for any particular form of STT.

Recognizing the importance of wall structure is but one of many considerations that must be applied when interpreting experiments. In a real system, pinning is always present, and the depinning process is more complex than these simple descriptions suggest. If both torque terms are present, they work in tandem to depin a wall [34,39]. The confining energy depends both on the form of the pinning potential and on the configuration of the wall within that potential. The simulated depinning of a wall from a notch in Ref. [39] showed that adiabatic torque shifted the wall in the potential well, effectively lowering the barrier (H_p in Eq. (10)) that the nonadiabatic force worked to overcome. The relative importance of the two torque terms in the depinning process depends on the depth of the potential well. This was brought out in those simulations by the pronounced nonlinearity of j_{th} versus bias field. Such nonlinearity has been seen in several experiments [40–43], though not analyzed in these terms.

Comparisons among experiments must also be mindful of time scales. At very short time scales, resonant effects can become important. It was found in Ref. [44] that fast-rising current steps could excite resonant oscillations of a wall in a potential well. Depending on the phase of the oscillation when the current was terminated, the stored momentum could assist the wall in escaping the well. This resonant depinning caused j_{th} to vary periodically with pulse length out to the damping time of the oscillations. At longer time scales, thermal activation becomes important. At fixed field or current, thermal fluctuations can help depin a wall with a probability that increases the longer one waits. Likewise, for a fixed observation time, the probability of depinning increases with increasing temperature, field, and, presumably, current. These behaviors were confirmed in the depinning studies of Ref. [9] for Co/Pt multilayers, but in Ref. [43] it was reported that j_{th} *increased* with increasing temperature. Treatment of thermal effects has only just begun, and much work remains if an accurate picture is to emerge.

3.2. Current-driven wall displacement and spin transfer efficiency

The depinning of a domain wall is a complicated process, intricately related to its internal structure and the potential that confines it. When current frees a wall from that potential, it begins to move. In many cases, this motion appears to be no less complex. The velocity of current-driven wall motion was first reported by Yamaguchi et al. [45]. Using magnetic force microscopy, they imaged the position of a vortex wall in a Permalloy wire before and after applying current pulses (~100–1000 ns in duration). Above $j_{th} = 6.7 \times 10^{11}\,A/m^2$ they observed a mean displacement that increased in proportion to pulse length, with a large stochastic variation about that mean. The average velocity during each pulse was quite low, about 3 m/s at $\sim 7 \times 10^{11}\,A/m^2$, implying a spin-flip efficiency $\varepsilon \equiv v/(\eta j) \sim 0.1$. They surmised that most of the transferred spin momentum had been absorbed by dissipative processes rather than by wall translation.

Similar experiments were carried out using spin-polarized scanning electron microscopy (SEM) [46], revealing similarly low spin transfer efficiency. These experiments likewise imaged walls before and after applying current pulses and found only small displacements. At $j = 2.2 \times 10^{12}\,A/m^2$, walls traveled at most ~3 μm, corresponding to average velocities of ~0.3 m/s over the 10 μs pulse duration (i.e., ~0.3% spin-flip efficiency). In addition to wall displacement, these authors obtained detailed images of the wall spin structure before and after applying current. They found that current not only displaced the walls, but also distorted their internal structures. Specifically, the as-initialized walls were of a vortex structure, but after a series of pulses, the vortex core was expelled laterally from the wall. The distorted transverse wall that remained was immobile at current densities capable of displacing the initial vortex wall.

In a variation on this theme, Meier et al. [47], again used high-resolution magnetic imaging to observe current-induced wall displacements, but at much shorter time scales. Aiming to limit heating during the pulse and to explore the initial-state motion, they used fast risetime pulses of ~1 ns duration. In this case, wall displacements corresponding to spin-flip efficiencies of up to ~40% were reported, though again with considerable pulse-to-pulse variation. The result was thought to suggest that the velocity at the leading edge of a pulse might be much larger than the velocity driven by steady-state current [47].

The experiments of Ref. [48] may help bridge the gap between these results. In that work, the authors measured the *time-resolved* displacement of a domain wall in response to long (several μs) current pulses. They observed displacements of several μm, similar to those in the Yamaguchi [45] and Klaüi [46] experiments. However, the wall moved only at the leading edge of the pulse, halting within less than 300 ns (the temporal resolution of the experiment) of the initial application of current. Had the average velocity been determined from the ratio of displacement to total pulse duration, a very low spin-transfer efficiency would yet again have been inferred. The velocity of the wall before stopping, however, reached at least 15 m/s, implying a spin-flip efficiency near 100% during its motion.

Interestingly, wall motion occurred not only at the beginning of the pulse, but also at its termination [48]. The magnitude and direction of the terminal "jumps" were stochastic, and amounted to additional displacements of up to ~2 μm. These jumps could suggest that the current applied a "holding torque", maintaining the wall in an otherwise unfavorable configuration. When current was removed, the wall would then be free to relax into a new energy minimum.

Such behavior is reminiscent of the predicted transient motion below the precessional threshold for $\beta = 0$ [49]. In this case when current is applied to a (transverse) domain wall, it immediately assumes a velocity $v = \eta j$. As the wall moves forward it cants, and if $j < j_{\rm th}^{\rm prec}$ (''intrinsic threshold'') the velocity rapidly decays to zero as the canting angle reaches equilibrium. When current returns to zero, so does the canting angle, and the wall springs back to its starting point.

There are two inconsistencies between this picture and experiments. First, the expected displacement is just tens of nanometers [49], in contrast to the thousands of nanometers observed. Second, in this idealized 1D picture, wall motion is reversible and current generates no final-state displacement.

To approach a quantitative description, we must return to two experimental realities: the true nature of the wall structure and the influence of a heterogeneous potential landscape. The transient displacement δx of a 1D wall induced by sub-threshold current [49] is a function of the wall canting angle, roughly $\delta x/\Delta \sim \varphi/\alpha$, to first order in φ. In all the above experiments, the wall was initially vortex, and φ must be replaced by the lateral vortex displacement δy. With $\beta = 0$, current displaces a vortex towards one edge. As it moves the wall moves forward until the ''gyrotropic force'' is balanced by the ''restoring force'', at which point motion will cease.

A quick but very rough estimate of the forward displacement δx corresponding to a vortex displacement δy might be made by comparing the forward and lateral wall velocities in Eqs. (7). In the case of an unconstrained wall, the result [29] is $v_{||} \sim v_{\perp}/(2\alpha)$ for appropriate wire dimensions, suggesting that 100 nm [47] vortex displacements might drive wall displacements of several μm, even for $\beta = 0$ below the precessional threshold. Whether this remains true when geometrical restoring forces are included requires a treatment far beyond our scope. However, the transient displacements due to current-induced wall distortion are clearly a function of wall structure, and a thorough treatment of this problem is a prerequisite for interpreting experiments.

The above (adiabatic) mechanism is not the only process consistent with the experiments, and even if it is the dominant driving mechanism (i.e., $\beta << \alpha$) it cannot fully explain the results. These transient displacements, induced below $j_{\rm th}^{\rm prec}$ in a $\beta = 0$ picture, are reversible: the wall returns to its initial configuration when current returns to zero. Any displacement remaining after a pulse would require a constraining potential to hold the wall as its stored momentum dissipated. Hence, the pinning potential would play a direct role in the motion.

The stochastic motion resulting from nonuniformity was highlighted in Ref. [47]: wall propagation appeared as a current-induced hopping from one pinning site to the next, likely a feature of most experiments with j near threshold. The process was explored with an accompanying micromagnetic simulation mimicking the experimental geometry. When current was applied, the wall moved forward in discrete jumps due to pinning by irregularities at the edges. Although the wall did not move uniformly, when it did move, it moved quickly, in some cases at up to 110 m/s. What was not pointed out was that current alone *could not drive the wall that fast*. With $\alpha = \beta$ in the simulation, the maximum *direct* contribution of j to the velocity is limited by $v = \eta j$ to ~25 m/s assuming the authors used the experimentally determined polarization. It is likely that, as a wall reaches the top of one potential well, the attractive potential of the next one drives it forward. In such cases, assigning meaning to the observed velocity is a difficult proposition.

3.3. Vortex displacement and gyrotropic forces

An important ingredient in understanding current-driven domain wall motion is understanding the motion of vortices. Current drives a vortex predominantly through a gyrotropic force, evidence for which has come from several experiments. The first was by Hung et al. [7], who imaged the current-driven motion of extended cross-tie walls in a Permalloy film. As predicted, current caused Bloch lines (vortices) to translate along the walls, normal to **j**, in a direction that depended on vortex polarity. Several recent experiments have revisited gyrotropic vortex motion in submicron structures. Two of these experiments [46,47], introduced in the previous section, involved imaging current-induced changes to the structure of vortex walls in nanowires. A third [50] measured the steady-state displacement, by dc current, of a vortex in a Permalloy disk. There are subtle but important differences between these experiments, which we explore here.

A vortex in a laterally confined structure tends to reside near the center of the structure due to a ''restoring'' force of magnetostatic origin [29]. In a wire, this force is proportional to the lateral displacement δy of the vortex core away from the center axis; i.e., $F_{\rm R} = -\kappa \delta y$, where κ is estimated in Ref. [29]. In a disk, δy is replaced by the radial displacement. Current subjects a vortex to two additional forces: a nonadiabatic force in the direction of electron flow and a gyrotropic force $F_y = G\eta j$ normal to **j**.

Consider first a vortex in static equilibrium, as occurs if restoring forces balance those due to current. Then the velocity terms in Ref. (7) vanish, leaving only the current-induced forces. The ratio of nonadiabatic to gyrotropic forces in Eq. (7) is $|F_x^j/F_y^j| = \beta w/\pi \Delta_{\rm eff}$, amounting to a few times β in typical experimental geometries. For reasonable estimates of β ($\ll 1$) the total current-induced force is thus dominantly gyrotropic, and the equilibrium vortex position corresponds to a displacement along y by an amount [51]

$$\delta y|_{v=0} \approx \frac{G}{\kappa}\eta j. \tag{11}$$

A nonadiabatic force, if present, contributes at most a very small correction. This case was realized in the experiment of Ref. [50], wherein current was injected

across a thin Permalloy disk. The disk magnetization was oriented tangentially in the plane, except for the small perpendicular "core" at its center. Using the Hall effect, correlated with Kerr magnetometry, the authors were able to resolve very small vortex displacements. The core was displaced either by a field or by current, and it returned reversibly to the center as long as the displacement was not too great. The displacement under current alone was close to that expected from Eq. (11) for κ appropriate to the geometry [50,51]. This experiment is perhaps the clearest observation to date of a current-induced gyrotropic force.

Consider now a vortex domain wall in a nanowire. If $\beta = 0$ or if the wall is pinned, we recover the case above. In equilibrium, the wall position is fixed with the vortex displaced toward one edge by an amount given by Eq. (11). If $\beta \neq 0$ and pinning is low, the wall moves forward while the vortex within it experiences another gyrotropic force, $\mathbf{F}_v = \mathbf{G} \times \mathbf{v}$. This force now acts with the current-induced gyrotropic force to determine the equilibrium lateral vortex displacement. If j is not too great, the wall moves uniformly forward at a velocity $v = (\beta/\alpha)\eta j$, with the vortex at

$$\delta y|_{v \neq 0} = \left(1 - \frac{\beta}{\alpha}\right) \frac{G}{\kappa} \eta j. \tag{12}$$

Note the difference in Eqs. (11) and (12). If the wall is not in motion, the vortex displacement is almost independent of β, but if it is in motion, β plays an important role.

In Refs. [46,47], vortex walls in nanowires were examined before and after the application of current pulses, and both reported forward motion coincident with lateral vortex displacement. A series of images in Ref. [47] showed a vortex moving progressively closer to the wire edge after each pulse, by an amount $\delta y = 83 \pm 36$ nm per pulse. On its surface, this seems a clear observation of gyrotropic force by the current on the vortex. Assuming so, the authors applied Eq. (12) and concluded $\beta/\alpha = 0.96 \pm 0.02$. If correct, this would be the most precise measurement of nonadiabicity to date. A closer look, however, raises many questions.

In Eq. (12), δy is the equilibrium displacement such that gyrotropic forces are balanced by the "restoring force" $F_R = -\kappa \delta y$. This force results from the change in wall energy due to a distortion of the wall, and can be approximated by a "force constant" $\kappa \approx K_u/\Delta$ [29]. The restoring force is a direct consequence of lateral confinement in the wire, and the latter formally enters through the shape contribution to K_u. Puzzlingly this contribution to K_u was neglected in Ref. [47], although at $\sim 4 \times 10^5$ erg/cm^3 (see Eq. (6)) it dwarfs the assumed 10^3 erg/cm^3 appropriate to induced anisotropy in a continuous film. With more appropriate constants in Eq. (12), $\delta y \sim 80$ nm would imply $\beta/\alpha \sim 400$, a rather astonishing result. Of course, such a high degree of nonadiabicity, if present, would be readily apparent elsewhere. For example, the current-induced force should easily overcome pinning, as per Eq. (10). With $\beta/\alpha \sim 400$ it would be difficult to explain the observed critical current of $\sim 1 \times 10^{12}$ A/m^2 [47], which would require pinning fields of several hundred Oe. Although the precise form of κ depends on the model of the wall, clearly, the picture leading to Eq. (12) cannot fully explain the experiment at hand. Because the wall "jumps" from pinning site to pinning site, its internal structure will relax around the local environment each time it moves. Whether internal wall distortions are driven directly by current or indirectly by the pinning potential cannot be unambiguously determined here.

3.4. Domain wall velocities, mobilities, and Walker breakdown

If one wants to know how a current drives a domain wall, one must know its dynamic state as it moves. The mobility curve $v(H)$ of a wall is a window into its dynamics, and the influence of current on wall dynamics is quite naturally explored through its effects on this curve. As we have seen, the motion of a domain wall is either viscous or precessional, with a current-dependent critical field separating these dynamical modes. In the viscous regime, wall velocity is augmented by current solely through the nonadiabatic term of Eq. (1). Once a wall is driven into precession, whether by field or by current, the adiabatic term takes over as the dominant contributor to net wall velocity. By measuring the dependence of v on j below and far above breakdown, both η and β/α can in principle be obtained *via* Eqs. (4). At the same time, the variation of H_w with j provides an independent gauge of β/α, via Eq. (3), assuming that η and μ are known and the underlying model is robust.

Experiments have shown current to have little effect on H_w, but to change significantly the field-driven velocity of a domain wall [36,37]. The dependence $v(j)$ was found in Ref. [36] to be nearly the same for $H < H_w$ and $H \gg H_w$, where nonadiabatic and adiabatic terms, respectively, should dominate. However, $v(j)$ exhibited a skewed quadratic character, qualitatively distinct from the behavior predicted in existing theories. Similar behavior was seen at high fields in Ref. [37], although the behavior below breakdown was unclear. The response of v to j could be decomposed into components linear and quadratic in j [36]. Interpreted in terms of Eqs. (4), the linear components yield $\eta = 2.7 \pm 0.1\, 10^{-11}$ m^3/C and $\beta/\alpha = 0.8 \pm 0.1$. At the same time, using the weak variation of H_w with j, about 0.5 Oe at 6×10^{11} A/m^2, along with the measured μ and η, Eq. (3) yields $\beta/\alpha = 0.6 \pm 0.2$.

Interpreted within the 1D model framework, analysis of velocities and Walker fields thus yields self-consistent results for the magnitude of nonadiabicity. However, these quantitative results must be viewed with caution. The 1D model predicts a zero-current breakdown field of ~ 100 Oe, much larger than the 6 Oe observed in Ref. [36]. Since the nonadiabatic component is analogous to a field, if the model fails to describe field-driven breakdown by an order of magnitude, it is questionable that variations in H_W can be reliably used to gauge the magnitude of β. Likewise,

adiabatic torque is an analog of the precessional damping that drives wall motion well above breakdown and leads to the high-field mobility. The 1D model predicts that the high-field mobility is lower by a factor $\alpha^2 \sim 10^{-4}$ than its low-field counterpart, compared to an observed reduction of only $\sim 10^{-1}$. Finally, even if the vortex dynamics are fully included in the model, it is not clear how a nonlinear dependence of v on j could arise. Resolving these points is critical to properly interpreting experiments.

4. Perspective on current-driven domain wall motion

We have covered experiments that reveal a rich array of behaviors by domain walls in response to spin-polarized electric current. The equation of motion (1), combined with an appropriate wall model, appears capable of describing most of these behaviors at least qualitatively. Does experimental agreement with Eq. (1) constitute progress in our understanding? Written in terms of unconstrained "fitting parameters" α, η, and β, it would be rather surprising if (1) *failed* to describe experiments: it is a very general accounting of torques, with the two spin-torque terms exhausting the possibilities of linearly introducing the gradient in **m** [14]. The first step in moving beyond this phenomenological picture requires putting constraints on its parameters.

4.1. Nonadiabatic torque: the beta question

The microscopic process behind adiabatic STT is relatively undisputed. Whether this is the only interaction between a spin-polarized current and a domain wall remains an open and very important question. As mentioned early on, one of the main differentiators of competing microscopic models is whether, and if so how, they introduce additional torque terms. Experimental discrimination amongst the models in large part comes down to quantifying β in Eq. (1). In Table 1 we summarize existing experimental estimates of this quantity. The most reliable results suggest $\beta \approx \alpha$. Whether this is a general feature, and if so why, remains to be seen. Estimates of the spin-flip scattering contribution to β [13], taken as the ratio of $\tau_{ex} = \hbar/J_{ex}$ to the spin-flip relaxation time give $\beta \sim 10^{-2}$, of the same order as α. Other estimates [52], however, cast doubt on any significant contribution at all for realistic domain wall widths. That these two "phenomenological" parameters might just happen to be equal may have more general implications. Stiles et al. [16] have pointed out that if one assumes adiabatic STT alone with Lifshitz-type damping, which is the preferred form in terms of thermodynamics, then $\beta \equiv \alpha$ in Eq. (1). In this picture, current appears as two terms in Eq. (1) simply because the (Lifshitz) damping term is written in a less natural way.

Table 1
Experimental estimates of nonadiabicity

Measurement	Ref.	Estimated β/α
Wall velocity ($H_p < H < H_w$)	[36]	0.8 ± 0.1
Walker breakdown field	[36]	0.6 ± 0.2
Walker breakdown field	[37]	1 ± 2[a]
Precessional frequency	[38]	1.6 ± 0.3[a]
Oscillatory depinning period	[44]	$8 \pm ?$
Vortex displacement	[47]	>400[b]

Summary of experimental estimates of nonadiabatic spin, torque in Permalloy nanowires.

[a]Estimates made here from published data using 1D model relations.

[b]Neglecting shape anisotropy, the analysis in Ref. [47] arrived at, $\beta/\alpha = 0.96 \pm 0.02$. See text for details.

It is still much to early to draw broad conclusions from the limited data. Experiments have reached the "proof-of-concept" stage of developing reliable means of quantifying the key parameters of Eq. (1). Realistic wall models and numerical simulations are still required to draw firm quantitative conclusions from the experiments. Moreover, "measuring" β is only the first step. Understanding its origin requires exploring its dependence on, for example, material properties and geometrical factors.

Finally, while it is tempting to dismiss effects beyond "spin-torque" when interpreting experiments, doing so must be done with rigor. A case in point is the oft-present statement to the effect "hydromagnetic domain drag effects are negligible for film thicknesses less than 100 nm". Justification is based on an early analysis by Berger [5] of the Hall-induced current loops circulating about a domain wall. A closer look shows that for the dimensions of many experiments, even a modestly large Hall coefficient, whose values are very sample-dependent [5] and often hard to come by, could generate significant effects. The reason they can be neglected in most nanowires is not necessarily because the wires are thin, but because the domains lie along **j**, removing the discontinuity in Hall voltage across a wall necessary for the effect. Consider, however, the current-driven depinning experiments of Refs. [9], on Co/Pt multilayers with perpendicular anisotropy. Based on the dimensions and separate measurements of the anomalous Hall effect [53], the analysis by Viret [54] would predict "domain-drag" forces yielding an effective "β" of more than 100α, comparable to what is implied by the experiment [9].

4.2. Other experimental considerations

We conclude by briefly outlining other possible impediments to unambiguously interpreting experiments. Experimental current thresholds tend to coincide with the onset of significant Joule heating. Incorporating temperature effects into the theoretical framework is nontrivial, but experimental consequences are abundantly clear. For example, Joule heating alone has been implicated in "current-induced" wall structure transformations and random wall jumps [55]. In addition, thermal time constants for metallic wires on Si are of the same order as relaxation times for domain wall processes. This could complicate attempts to

resolve the transient response of a domain wall to a current pulse. Oersted field effects have also received incomplete treatment. In nanowire geometries, the Oersted field circulates about the wire axis, lacking a longitudinal component that could drive wall motion. For this reason, it is often neglected. However, the normal field component, which can reach 100 Oe, is not uniform and changes direction from one side of a planer wire to the other. It seems premature to exclude the possibility of nontrivial effects due to this gradient. For example, if the field slightly tips the wall plane or displaces a vortex, it could significantly effect wall depinning. These are but a few of the many issues that must be addressed as our experimental understanding matures.

Acknowledgments

Work supported in part by the NSF-NIRT program (DMR-0404252) and the R.A. Welch Foundation (F-1015). The authors gratefully acknowledge important experimental contributions by C. Knutson, C. Nistor, and S. Yang.

References

[1] L. Berger, J. Appl. Phys. 49 (1978) 2156.
[2] L. Berger, J. Appl. Phys. 55 (1984) 1954.
[3] L. Berger, Phys. Rev. B 33 (1986) 1572.
[4] L. Berger, J. Appl. Phys. 63 (1988) 1663.
[5] P.P. Freitas, L. Berger, J. Appl. Phys. 57 (1985) 1266.
[6] C.-Y. Hung, L. Berger, J. Appl. Phys. 63 (1988) 4276.
[7] C.-Y. Hung, L. Berger, C.Y. Shih, J. Appl. Phys. 67 (1990) 5941.
[8] M. Yamanouchi, D. Chiba, F. Matsukura, H. Ohno, Nature 428 (2004) 539.
[9] D. Ravelosona, et al., Phys. Rev. Lett. 95 (2005) 117203.
[10] A.P. Malozemoff, J.C. Slonczewski, Magnetic Domain Walls in Bubble Materials, Academic Press, New York, 1979.
[11] G. Tatara, H. Kohno, Phys. Rev. Lett. 92 (2004) 086601.
[12] Z. Li, S. Zhang, Phys. Rev. Lett. 92 (2004) 207203.
[13] S. Zhang, Z. Li, Phys. Rev. Lett. 93 (2004) 127204.
[14] A. Thiaville, et al., Europhys. Lett. 69 (2005) 990.
[15] S.E. Barnes, S. Maekawa, Phys. Rev. Lett. 95 (2005) 107204.
[16] M. Stiles, W.M. Saslow, M.J. Donahue, A. Zangwill, Phys. Rev. B 75 (2007) 214423.
[17] R.D. McMichael, et al., IEEE Trans. Magn. 33 (1997) 4167.
[18] Y. Nakatani, A. Thiaville, J. Miltat, J. Magn. Magn. Mater. 290–291 (2005) 750.
[19] M. Laufenberg, et al., Appl. Phys. Lett. 88 (2006) 052507.
[20] N.L. Schryer, L.R. Walker, J. Appl. Phys. 45 (1974) 5406.
[21] G.S.D. Beach, C. Knutson, M. Tsoi, J.L. Erskine, J. Magn. Magn. Mater. 310 (2007) 2038.
[22] A.A. Aharoni, J. Appl. Phys. 83 (1998) 3432.
[23] G.S.D. Beach, C. Nistor, C. Knutson, M. Tsoi, J.L. Erskine, Nat. Mater. 4 (2005) 741.
[24] G.S.D. Beach, et al., unpublished.
[25] Y. Nakatani, et al., Nat. Mater. 2 (2003) 521.
[26] M.R. Scheinfein, LLG Micromagnetic Simulator™ 〈http://llgmicro.home.mindsrping.com〉.
[27] C. Nistor, et al., unpublished.
[28] A.A. Thiele, Phys. Rev. Lett. 30 (1973) 230.
[29] J. He, Z. Li, S. Zhang, Phys. Rev. B 73 (2006) 184408.
[30] O. Tchernyshyov, G.-W. Chern, Phys. Rev. Lett. 95 (2005) 197204.
[31] D. Clarke, G.-W. Chern, O.A. Tretiakovz, O. Tchernyshyov, 2007, arXiv:0705.4465.;
O.A. Tretiakov, Ya.B. Bazaliy, O. Tchernyshyov, 2007, arXiv:0705.4463.
[32] A. Yamaguchi, K. Yano, H. Tanigawa, S. Kasai, T. Ono, Japan J. Appl. Phys. 45 (2006) 3850.
[33] S.-M. Seo, et al., Appl. Phys. Lett. 90 (2007) 252508.
[34] G. Tatara, et al., J. Phys. Soc. Japan 75 (2006) 064708.
[35] L. Berger, Phys. Rev. B 73 (2006) 014407.
[36] G.S.D. Beach, et al., Phys. Rev. Lett. 97 (2006) 057203.
[37] M. Hayashi, et al., Phys. Rev. Lett. 96 (2006) 207205.
[38] M. Hayashi, et al., Nat. Phys. 3 (2007) 21.
[39] J. He, Z. Li, S. Zhang, J. Appl. Phys. 98 (2005) 016108.
[40] M. Kläui, et al., Appl. Phys. Lett. 83 (2003) 105.
[41] T. Kimura, Y. Otani, I. Yagi, K. Tsukagoshi, y. Aoyagi, J. Appl. Phys. 94 (2003) 7226.
[42] N. Vernier, D.A. Allwood, D. Atkinson, M.D. Cooke, R.P. Cowburn, Europhys. Lett. 65 (2004) 526.
[43] M. Laufenberg, et al., Phys. Rev. Lett. 97 (2006) 046602.
[44] L. Thomas, et al., Nature 443 (2006) 197.
[45] A. Yamaguchi, et al., Phys. Rev. Lett. 92 (2004) 077205;
A. Yamaguchi, et al., Phys. Rev. Lett. 96 (2006) 179904.
[46] M. Kläui, et al., Phys. Rev. Lett. 95 (2005) 026601.
[47] G. Meier, et al., Phys. Rev. Lett. 98 (2007) 187202.
[48] S. Yang, J.L. Erskine, Phys. Rev. B 75 (2007) 220403(R).
[49] Z. Li, S. Zhang, Phys. Rev. B 70 (2004) 024417.
[50] T. Ishida, T. Kimura, Y. Otani, Phys. Rev. B 74 (2006) 014424.
[51] J. Shibata, Y. Nakatani, G. Tatara, H. Kohno, Y. Otani, Phys. Rev. B 73 (2006) 020403(R).
[52] J. Xiao, Z. Zangwill, M.D. Stiles, Phys. Rev. B 73 (2006) 054428.
[53] C.L. Canedy, X.W. Li, G. Xiao, Phys. Rev. B 62 (2000) 508.
[54] M. Viret, A. Vanhaverbeke, F. Ott, J.-F. Jacquinot, Phys. Rev. B 72 (2005) 140403(R).
[55] F. Junginger, et al., Appl. Phys. Lett. 90 (2007) 132506.